

The Aquarius Salinity Retrieval Algorithm

Thomas Meissner and Frank Wentz

Remote Sensing Systems
Santa Rosa, CA, USA

meissner@remss.com, frank.wentz@remss.com

Gary Lagerloef

Earth and Space Research
Seattle, WA, USA

David Le Vine

NASA's Goddard Space Flight Center
Greenbelt, MD, USA

Abstract— This paper gives an overview of the algorithm for retrieving sea surface salinity from the AQUARIUS L-band radiometer and its physical background.

Keywords— Aquarius, Sea surface salinity, L-band radiometers, sea surface roughness.

I. BACKGROUND

The Aquarius L-band radiometer/scatterometer system is designed to provide monthly salinity maps at 150 km spatial scale to an accuracy of 0.2 psu [1]. The sensor was launched on June 10, 2011, aboard the Argentine CONAE SAC-D spacecraft. The L-band radiometers and the scatterometer have been taking science data observations since August 25, 2011.

II. OVERVIEW OF THE AQUARIUS LEVEL 2 PROCESSING

This section gives an overview over the Aquarius salinity retrieval algorithm.

The instrument calibration [2] converts Aquarius radiometer counts into antenna temperatures (TA). The salinity retrieval algorithm converts those TA into brightness temperatures (TB) at a flat ocean surface and sea surface salinity (SSS). As a first step, contributions arising from the intrusion of solar, lunar and galactic radiation are subtracted. The antenna pattern correction (APC) removes the effects of cross-polarization contamination and spillover. The Aquarius radiometer measures the 3rd Stokes parameter in addition to vertical (v) and horizontal (h) polarizations, which allows for an easy removal of ionospheric Faraday rotation. The atmospheric absorption at L-band is almost entirely due to molecular oxygen, which can be calculated based on auxiliary input fields from numerical weather prediction models (e.g. NCEP) and then successively removed from the TB. The final step in the TA to TB conversion is the correction for the roughness of the sea surface due to wind, which is addressed in more detail in section III.

The TB of the flat ocean surface can now be matched to a salinity value using a surface emission model that is based on a model for the dielectric constant of sea water [3], [4] and an auxiliary field for the sea surface temperature. In the current processing only v-pol TB are used for this last step.

III. MODEL FOR THE EMISSION OF WIND ROUGHENED OCEAN SURFACE AT L-BAND

One of the major error sources in the Aquarius salinity retrieval is the change in the ocean surface emissivity due to roughening by wind.

A. Wind Speed Dependence

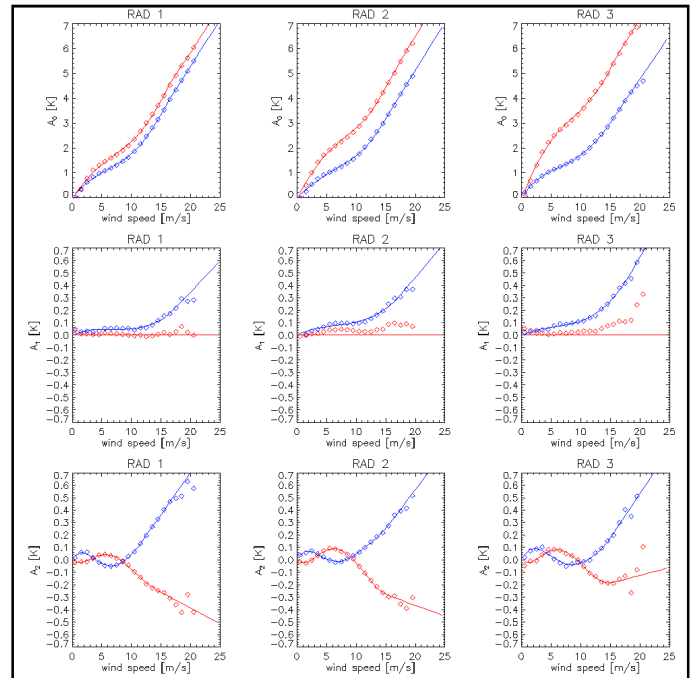


Figure 1: Harmonic coefficients of the expansion (1) of the wind induced surface brightness temperature $\Delta E_w \cdot T_s$ (in Kelvin) for the 3 Aquarius radiometers: blue = v-pol, red=h-pol. The Earth incidence angles for the beams are: 28.7° (RAD 1), 37.9° (RAD 2) and 45.5° (RAD 3).

A model for the wind induced emissivity has been developed post-launch based on actual Aquarius observations. As a first step, Aquarius brightness surface brightness temperatures were collocated with surface wind speed and wind direction measurements from NCEP, SSMIS F17 and WindSat, from

which the harmonic coefficients A_i , $i=0,1,2$ of the wind induced emissivity ΔE_w can be derived:

$$\Delta E_w(W, \varphi_r) \cdot T_s = A_0(W) + A_1(W) \cdot \cos(\varphi_r) + A_2(W) \cdot \cos(2\varphi_r) \quad (1)$$

W is the surface wind speed, φ_r is the surface wind direction relative to the looking azimuth and T_s is the sea surface temperature. The results for the 3 Aquarius horns are shown in Figure 1. This allows performing a roughness correction based on auxiliary wind speed and wind direction fields from NCEP.

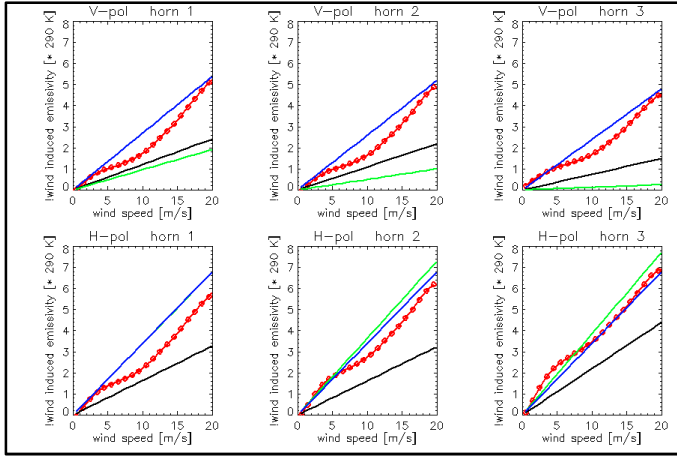


Figure 2: Comparison of the wind induced surface brightness temperature $\Delta E_w \cdot T_s$ [$\cdot 290$ Kelvin] from Aquarius (red) with the results of [5] (black), [6] (green) and [7] (blue).

Figure 2 compares the L-band wind induced surface brightness temperature as function of wind speed from Aquarius with other measurements.

B. Roughness and Scatterometer Backscatter

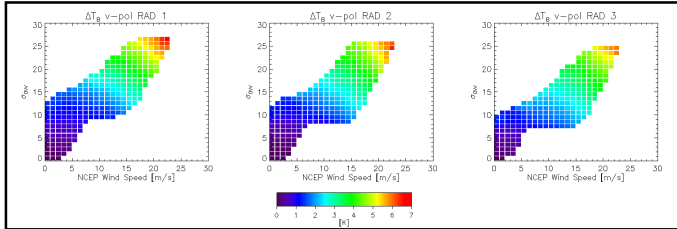


Figure 3: The wind induced surface brightness temperature $\Delta E_w \cdot T_s$ [$\cdot 290$ Kelvin] binned with respect to surface wind speed from NCEP W_{NCEP} and the scatterometer measurement $\sigma_{0,VV}$. The $\sigma_{0,VV}$ has been scaled to units of wind speed [m/s]. The wind direction signal has been removed from both $\Delta E_w \cdot T_s$ and $\sigma_{0,VV}$.

As a next step the radar backscatter cross section measurements σ_0 of the Aquarius scatterometer can be used in addition to NCEP wind speed and direction in order to improve the roughness correction. Both, radiometer and scatterometer observation need to be first corrected for wind direction, which is done based on the functions from Figure 1 and an analogous analysis for σ_0 . The wind induced emissivity can be parameterized and calculated from a lookup table containing

both NCEP wind speed W_{NCEP} and the σ_0 for the vv-pol backscatter. The results are shown in Figure 3.

C. Surface Roughness Correction

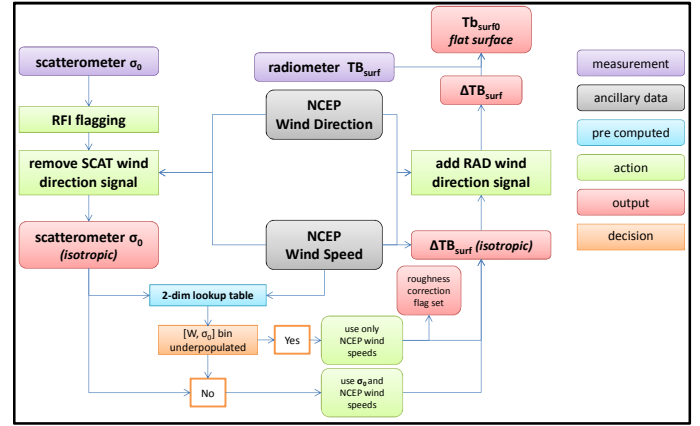


Figure 4: Schematic flow of the surface roughness correction algorithm.

Figure 4 shows the flow of the algorithm that correcting for the surface roughness. If the $[W_{NCEP}, \sigma_{0,VV}]$ bin in the 2-dimensional lookup table (Figure 3) is underpopulated, only W_{NCEP} is used in the roughness correction.

IV. FIRST RESULTS FOR SEA SURFACE SALINITY

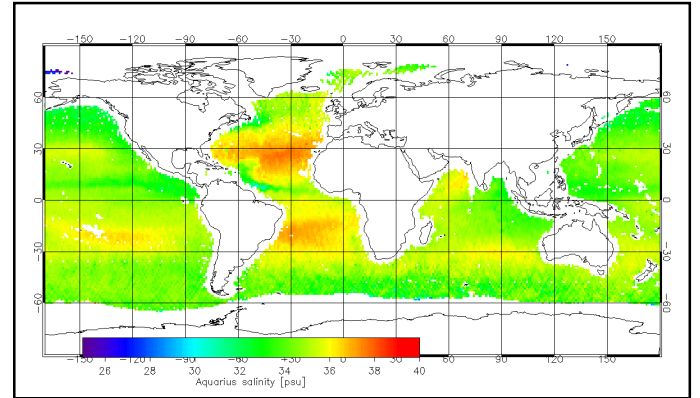


Figure 5: Aquarius salinity map for the month of September 2011.

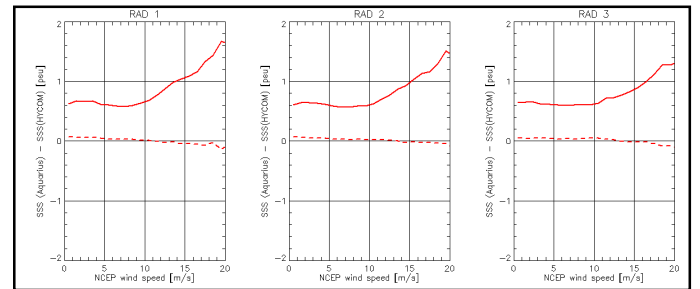


Figure 6: Statistics of Aquarius versus HYCOM salinity (SSS) as function of NCEP wind speed: dashed line = bias, full lines = standard deviation.

Figure 5 shows a map of the retrieved Aquarius salinity from all 3 horns for September 2011. The results for a statistical comparison between Aquarius and HYCOM salinity fields are shown in Figure 6 (as function of NCEP wind speed) and Figure 7 (as function of SST).

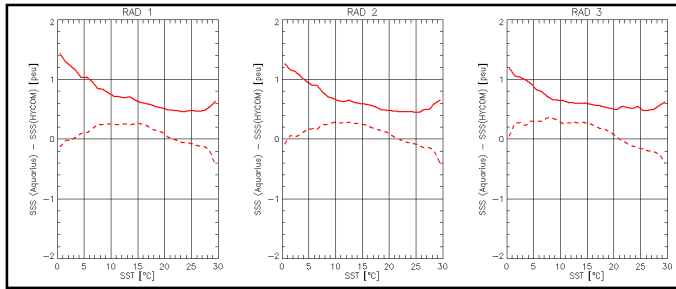


Figure 7: Statistics of Aquarius versus HYCOM salinity (SSS) as function of SST: dashed line = bias, full lines = standard deviation.

REFERENCES

- [1] D. M. Le Vine, G. S. Lagerloef, F. R. Colomb, S. H. Yueh, and F. A. Pellerano, "Aquarius: An instrument to monitor sea surface salinity from space," *IEEE Trans. Geosci. Remote Sens.*, vol. 44, no. 7, pp. 2040 - 2050, 2007.
- [2] J. R. Piepmeier, "Calibration of Passive Microwave polarimeters that Use Hybrid Coupler-Based Correlators," *IEEE Trans. Geosci. Remote Sens.*, vol. 42, no. 2, pp. 391 - 400, 2004.
- [3] T. Meissner and F. J. Wentz, "The complex dielectric constant of pure and sea water from microwave satellite observations," *IEEE Trans. Geosci. Remote Sens.*, vol. 42, no. 9, pp. 1836 - 1849, 2004.
- [4] T. Meissner and F. J. Wentz, "The emissivity of the ocean surface between 6 and 90 GHz over a large range of wind speeds and Earth incidence angles," *IEEE Trans. Geosci. Remote Sens.*, 2012, in print.
- [5] J. P. Hollinger, "Passive microwave measurements of sea surface roughness," *IEEE Trans. Geosc. Electr.*, vol. 9, pp. 165 - 169, 1971.
- [6] C. Gabarro, M. Vall-Llossera, J. Font and A. Camp, "Determination of sea surface salinity and wind speed by L-band microwave radiometry from a fixed platform," *Int. J. Rem. Sens.*, vol. 25, no. 1, pp. 111 -128, 2004.
- [7] S. H. Yueh, S. J. Dinardo, A. H. Fore and F. K. Li, "Passive and active L-band microwave observations and modeling of ocean surface winds," *IEEE Trans. Geosci. Remote Sens.*, vol. 48, no. 8, pp. 3087 - 3100, 2010.